Microstructure and Soft Magnetic Properties of Nanocrystalline Fe–Zr–B–Al, Fe–Zr–B–Si and Fe–Zr–B–Al–Si Alloys with Zero Magnetostriction

Akihisa Inoue*, Yoshihiro Miyauchi*†, Akihiro Makino**
and Tsuyoshi Masumoto*

Institute for Materials Research, Tohoku University, Sendai 980-77, Japan
***Central Research Laboratory, Alps Electric Co. Ltd., Nagaoka 940, Japan**

An amorphous phase was formed in the composition ranges of Al or Si up to 15 at% for rapidly solidified $Fe_{91-x}Zr_7B_2Al_x$, $Fe_{90-x}Zr_7B_3Al_x$, $Fe_{91-x}Zr_7B_2Si_x$, $Fe_{90-x}Zr_7B_3Si_x$, $Fe_{91-x-y}Zr_7B_2Al_xSi_y$ and $Fe_{90-x-y}Zr_7B_3Al_xSi_y$ alloys. These amorphous alloys crystallize through two stages of Am→bcc-Fe+Am→α-Fe+Fe$_3$B. The first and second reaction temperatures are 773 to 923 K and 973 to 1073 K respectively. The annealing in the temperature range between the first and the second stages caused the formation of a nanoscale bcc structure in coexistence with the amorphous phase. The average particle size and interparticle spacing of the bcc phase in $Fe_{88}Zr_7B_3Al_2$ and $Fe_{86}Zr_7B_3Si_4$ alloys are about 15 nm and 10 nm, respectively, and the analytical compositions are 2 to 4 at%Zr and 3 at%Al or 6 at%Si for the bcc phase and 11 at%Zr and 1 at%Al or 3 at%Si for the remaining amorphous phase. The enrichment of Zr in the remaining amorphous phase causes the increase in the thermal stability of the amorphous phase which enables the formation of the nanoscale bcc structure in the wide temperature range. The magnetostriction (λ_s) value of the bcc Fe–Zr–B–Al, Fe–Zr–B–Si and Fe–Zr–B–Al–Si alloys as a function of Al and/or Si content changes from negative to positive value through zero around Fe–Zr–B–2%Al, Fe–Zr–B–4%Si and Fe–Zr–B–2%Si–1%Al. The permeability (μ_e) shows a maximum value at the composition where the zero λ_s is obtained and the highest μ_e at 1 kHz and saturation magnetization (B_s) are 1.6×10^4 and 1.61 T, respectively, for $Fe_{89}Zr_7B_2Al_2$, 1.4×10^4 and 1.56 T, respectively, for $Fe_{87}Zr_7B_2Si_4$ and 1.2×10^4 and 1.55 T, respectively, for $Fe_{88}Zr_7B_2Si_2Al_1$. The annealing temperature (T_a) range where the characteristics of $\lambda_s \sim 0$, $\mu_e > 10^4$ and $B_s > 1.5$ T are achieved is also extended from about 20 K for the Fe–Zr–B alloy to about 100 to 130 K for the 2 at%Al or 4 at%Si alloy. The zero λ_s for the 2 at%Al or 4 at%Si alloy is related to the simultaneous dissolution of Zr and Al or Si in the nanoscale bcc phase. The simultaneous achievement of zero λ_s, high μ_e and high B_s in the wide T_a range through the dissolution of more than two solute elements in the bcc phase and the redistribution of solute elements between the bcc and amorphous phases is important for future development of the present magnetic alloys.

(Received July 14, 1995)

Keywords: nanocrystalline alloy, iron base alloy, nanoscale bcc phase, nanocrystallization, soft magnetic alloy, high saturation magnetization, zero magnetostriction, rapid solidification, amorphous phase

1. Introduction

Recently, nanocrystalline Fe-based alloys prepared by crystallization of a rapidly solidified amorphous phase have attracted increasing interest as a new type of magnetic materials which show useful magnetic properties, e.g., soft and/or hard and high magnetostrictive property with high sensitivity at low magnetic fields[1]. When we pay attention to the nanocrystalline alloys, good soft magnetic properties with a high permeability (μ_e) exceeding 1×10^4 at 1 kHz and a high saturation magnetization (B_s) above 1.2 T have been obtained in the Fe–Si–B–Nb–Cu[2], Fe–M–B (M=Zr, Hf, Nb)[3][4] and Fe–Si–B–Nb–Ga[5] systems. The highest combined characteristics of μ_e and B_s have been reported to be 1.2×10^5 and 1.2 T for the Fe–Si–B–Nb–Cu system, 1.0×10^5 and 1.6 T for the Fe–Zr–Nb–B system[6] and 1.0×10^4 and 1.2 T for the Fe–Si–B–Nb–Ga system. From these fundamental characteristics, one can notice that the Fe–M–B (M=Zr, Hf, Nb)

nanocrystalline alloys are extremely attractive for the application to power transformers because of the much higher B_s values than those for the other nanocrystalline soft magnetic alloys. However, the nanocrystalline alloys in Fe–M–B ternary and quaternary systems have slightly negative magnetostriction (λ_s) even at an optimum annealing condition where the best combined characteristics of μ_e and B_s are obtained[3][4]. The modification of λ_s from the slightly negative to zero value is expected to cause further increase in μ_e. Additionally, the nanocrystalline structure has been reported to consist of bcc Fe(Si) and remaining amorphous phase for the Fe–Si–B–Nb–Cu system[7], and bcc-Fe and remaining amorphous phase for the Fe–M–B system[8]. Thus, the primary crystalline phase leading to the good soft magnetic properties is the bcc-Fe phase containing about 22 to 25 at% Si for the former system and a nearly pure bcc-Fe phase without appreciable solute elements for the latter system. The significant compositional difference in the bcc-Fe phases between the above two alloy systems allows us to expect that the dissolution of an optimum amount of solute element into the nearly pure bcc-Fe phase causes fur-

---

† On leave from Nippon Denko Co. Ltd., Tokyo 104, Japan.

ther improvement of the soft magnetic properties of the nanocrystalline Fe-M-B alloys. From these scientific points of view, we have performed a systematic study on the effect of a small amount of additional element on the achievement of zero magnetostriction for the nanocrystalline Fe-Zr-B alloys. As a result, we have found that the addition of a small amount of Al and/or Si to the Fe-Zr-B alloys is effective in achieving a nearly zero magnetostriction and an improvement of μ_e. Although a part of the results in the nanocrystalline Fe-Zr-B-Si alloys have been presented as a short paper[9], this paper is intended to present the details of the microstructure and soft magnetic properties of nanocrystalline Fe-Zr-B-Al, Fe-Zr-B-Si and Fe-Zr-B-Al-Si alloys prepared by partial crystallization of their melt-spun amorphous alloy ribbons and to investigate the relation between the solute concentrations in the bcc-Fe and remaining amorphous phases and the achievement of zero λ_s.

II. Experimental Procedure

Alloy ingots in the $Fe_{91-x}Zr_7B_2Al_x$, $Fe_{90-x}Zr_7B_3Al_x$, $Fe_{91-x}Zr_7B_2Si_x$ and $Fe_{90-x}Zr_7B_3Si_x$ ($x=1$ to 15 at%) quaternary and $Fe_{91-x-y}Zr_7B_2Al_xSi_y$ and $Fe_{90-x-y}Zr_7B_3Al_xSi_y$ (x or $y=1$ to 5 at%) penternary systems were produced by arc melting mixtures of pure iron, zirconium and aluminum metals with purities above 99.9 mass% and pure silicon (99.999 mass%) and boron (99.8 mass%) crystals in an argon atmosphere. The subscripts represent the nominal atomic percentage of the mixtures. Rapidly solidified ribbons with a cross section of about 0.02×1 mm^2 were produced in an argon atmosphere by a single-roller melt spinning method in which the copper roller with a diameter of about 200 mm is rotated at a constant circumferential speed of 42 m/s. The as-quenched samples were subjected to heating for 3.6 ks at various temperatures ranging from 573 to 1023 K inside a vacuum-sealed quartz tube, followed by water quenching.

As-quenched and annealed structures were examined by X-ray diffractometry using Cu Kα raidiation and conventional and high-resolution transmission electron microscopy (TEM). Alloy compositions in each constituent phase were also determined by using a nanobeam energy dispersive X-ray (EDX) spectroscope which was set in a high-resolution type transmision electron microscope (JEM-2010F). The thin foils for TEM observation were made by polishing electrolytically at approximately 223 K in a solution consisting of 90% ethanol and 10% perchloric acid in volume ratio. The decomposition behavior upon continuous heating at a rate of 0.17 K/s was also examined by differential scanning calorimetry (DSC). Magnetization under an applied field of 800 kA/m was measured at room temperature with a vibrating sample magnetometer. Effective permeability at 1 kHz under 0.8 A/m was evaluated with a vector impedance analyzer. In addition, magnetostriction was measured in an applied field up to 240 kA/m by a three-terminal capacitance method.

III. Results

1. Formation and crystallization behavior of amorphous Fe-Zr-B-Al and Fe-Zr-B-Si alloys

Figures 1 and 2 show the X-ray diffraction patterns of rapidly solidified $Fe_{90-x}Zr_7B_3Al_x$ and $Fe_{90-x}Zr_7B_3Si_x$ ($x=0$, 5, 10 and 15 at%) alloys, respectively. All the diffraction patterns consist of a broad halo peak with the maximum at a wave vector ($K_p=4\pi\sin\theta/(\lambda)$) of about
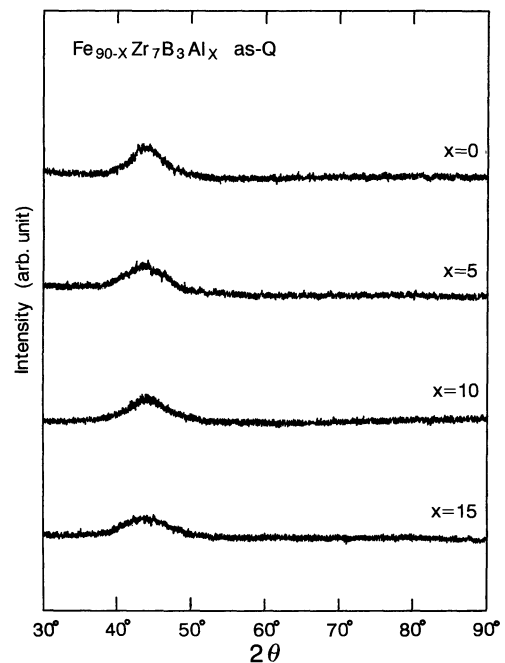

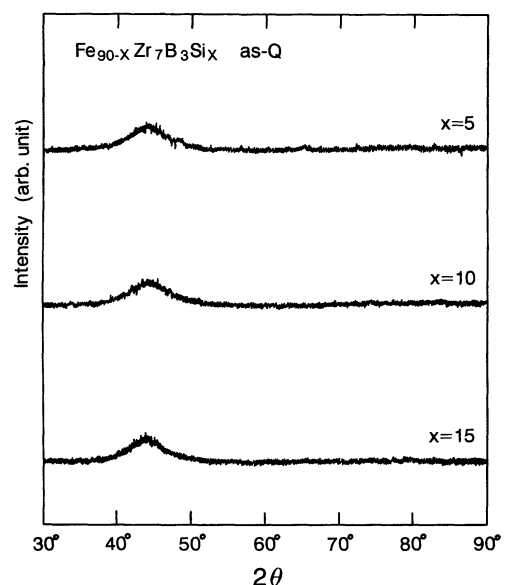Fig. 1   X-ray diffraction patterns of rapidly solidified $Fe_{90-x}Zr_7B_3Al_x$ ($x=0$, 5, 10 and 15 at%) alloys.

Fig. 2   X-ray diffraction patterns of rapidly solidified $Fe_{90-x}Zr_7B_3Si_x$ ($x=5$, 10 and 15 at%) alloys.

$30.4 \, \text{nm}^{-1}$ and no appreciable diffraction peaks corresponding to a crystalline phase is seen. These results indicate that an amorphous single phase is formed in the entire composition range up to 15 at% Al or Si. Thus, the fact that the glass-forming ability is almost unchanged by the replacement of Fe by Al or Si up to 15 at% is important for future development of Fe–Al and Fe–Si base amorphous alloys. In order to confirm the formation of an amorphous single phase, the bright-field electron micrographs and selected-area electron diffraction patterns of the rapidly solidified $Fe_{85}Zr_7B_3Al_5$ and $Fe_{85}Zr_7B_3Si_5$ alloys are observed as shown in Fig. 3. The bright-field images reveal the featureless contrast for both alloys and the diffraction patterns consist only of halo rings. It is thus concluded that the rapidly solidified Fe–Zr–B–Al and Fe–Zr–B–Si alloys are composed of an amorphous phase without any crystallinity. Here, it is important to point out that the critical sample thickness for the formation of an amorphous single phase is considerably larger for the Fe–Zr–B–Al and Fe–Zr–B–Si alloys than for the $Fe_{90}Zr_7B_3$ alloy, though no appreacible change in good bending ductility is seen for both alloy systems. That is, the critical thickness was measured to be about 26 μm for the $Fe_{88}Zr_7B_3Al_2$ alloy, 28 μm for the $Fe_{86}Zr_7B_3Si_4$ alloy, being larger than about 18 μm for the $Fe_{90}Zr_7B_3$ alloy.

Figure 4 shows the DSC curves of the $Fe_{89}Zr_7B_2Al_2$ and $Fe_{88}Zr_7B_3Al_2$ amorphous alloys. It is seen that two exothermic peaks appear in the temperature ranges of 780 to 840 K and 1020 to 1040 K, indicating that the crystallization takes place through two stages. Furthermore, the heat of exothermic reaction of the first stage is much larg-

er than that of the second stage. We examined crystalline phases corresponding to the two exothermic reactions by X-ray diffractometry. Figure 5 shows the X-ray diffraction patterns of the amorphous $Fe_{88}Zr_7B_3Al_2$ alloy annealed for 3.6 ks at 823, 923 and 1073 K corresponding to the temperatures marked with A, B and C, respectively, in Fig. 4, together with the data of the as-quenched sample. The diffraction peaks are identified to consist of amorphous + bcc-Fe phases for the sample annealed at 823 K, a mostly single bcc-Fe phase at 923 K and α-Fe + cubic Fe_3Zr at 1073 K. The lattice parameter of the bcc-Fe phase is measured to be 0.2874 nm at the annealing temperature (T_a) of 823 K, 0.2872 nm at 923 K and
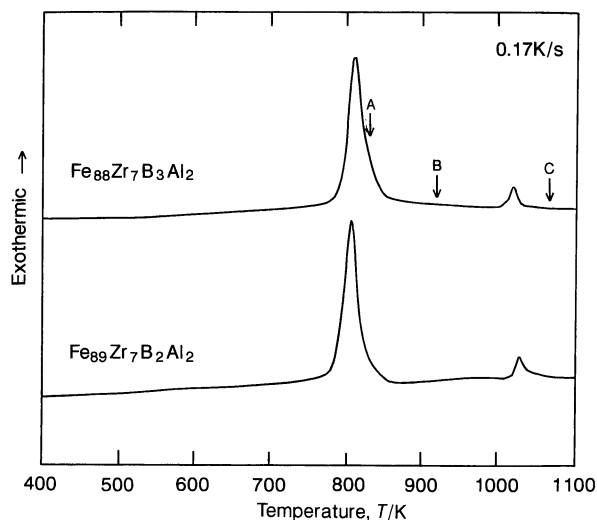
Fig. 4 Differential scanning calorimetric (DSC) curves of amorphous $Fe_{89}Zr_7B_2Al_2$ and $Fe_{88}Zr_7B_3Al_2$ alloys.

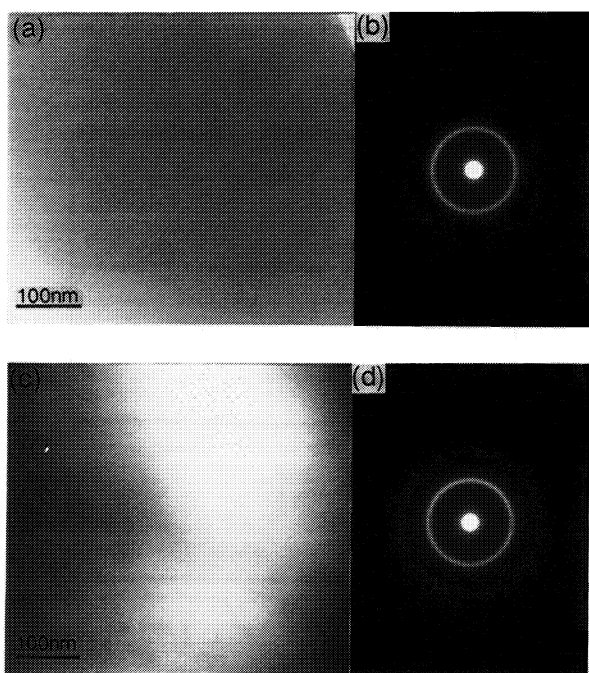Fig. 3 Bright-field electron micrographs and selected-area electron diffraction patterns of rapidly solidified $Fe_{86}Zr_7B_2Al_5$ (a and b) and $Fe_{86}Zr_7B_2Si_5$ (c and d) alloys.
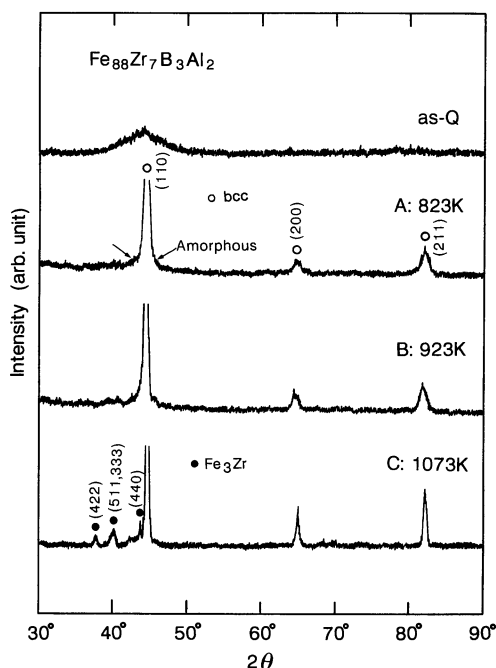
Fig. 5 DSC curves of amorphous $Fe_{87}Zr_7B_2Si_4$ and $Fe_{86}Zr_7B_3Si_4$ alloys.

0.2869 nm at 1073 K. There is a tendency for the lattice parameter of the bcc-Fe phase to decrease with increasing T_a. These lattice parameters are larger than that (0.28664 nm)[10] of pure α-Fe, indicating that the bcc-Fe phase is a solid solution enriched with the solute elements (mainly Al and B). The monotonous decrease in the lattice parameter with increasing T_a is due to the gradual elimination of the solute elements from the bcc-Fe phase to the remaining amorphous phase. This result indicates that the first-stage exothermic peak with high intensity is due to the precipitation of a primary bcc-Fe phase and the second-stage exothermic peak with low intensity results from the transition to α-Fe + Fe_3Zr phases. No appreciable diffraction peaks corresponding to Fe_3Al, Al_3Zr, Fe_3B and Fe_2B are seen. Consequently, the small amounts of Al and B elements are thought to be dissolved into the α-Fe phase for Al and the Fe_3Zr phase for B, because a large amount of Al can be dissolved into bcc-Fe phase in an equilibrium state[11] and B element has strongly attractive bonding nature against Fe and Zr elements[12]. Thus, the crystallization process of the Fe-Zr-B-Al amorphous alloys can be represented as follows; Am→Am + bcc-Fe→α-Fe + Fe_3Zr.

The similar crystallization behavior was also recognized for the amorphous Fe-Zr-B-Si alloys. Figure 6 shows the DSC curves of the amorphous $Fe_{87}Zr_7B_2Si_4$ and $Fe_{86}Zr_7B_3Si_4$ alloys. Two exothermic peaks are seen in the temperature ranges of 790 to 840 K and 1050 to 1070 K, indicating that these Fe-Zr-B-Si amorphous alloys crystallize through two stages. Furthermore, the $Fe_{86}Zr_7B_3Si_4$ alloy annealed for 3.6 ks at 923 K corresponding to the temperature between the first- and second-exothermic peaks consists of coexistent amorphous and bcc-Fe phases, as shown for the X-ray diffraction patterns in Fig. 7. The increase in T_a to the temperature just above the second exothermic peak causes the precipitation of Fe_3Zr. As similar to that for the Fe-Zr-B-Al amorphous alloys, no appreciable diffraction peaks

corresponding to Fe_3Si, Fe_2Si, Fe_3B and Fe_2B phases are seen in the X-ray diffraction patterns shown in Fig. 7. It is thus concluded that the Fe-Zr-B-Si amorphous alloys have the crystallization process of Am→Am + bcc-Fe→α-Fe + Fe_3Zr. Here, it is important to point out the reason why the Fe-based alloys containing 2 at% Al or 4 at% Si were chosen. It is due to the achievement of
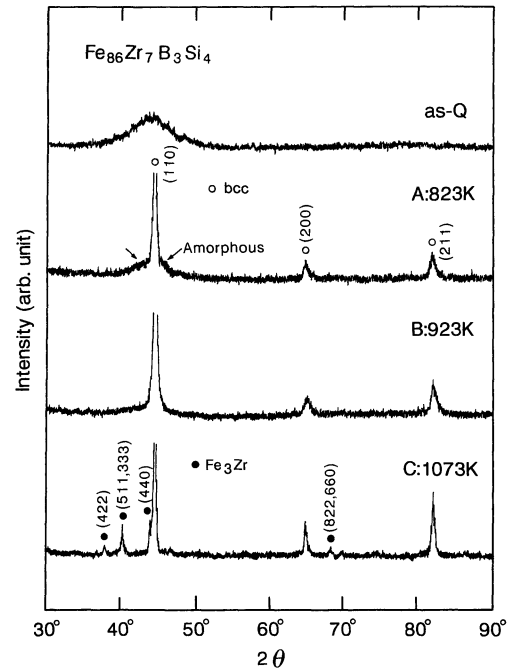

Fig. 7 X-ray diffraction patterns of an amorphous $Fe_{86}Zr_7B_3Si_4$ alloy annealed for 3.6 ks at various temperatures.
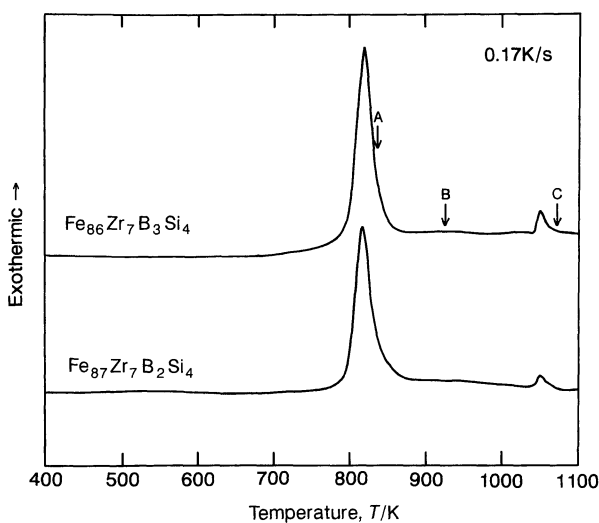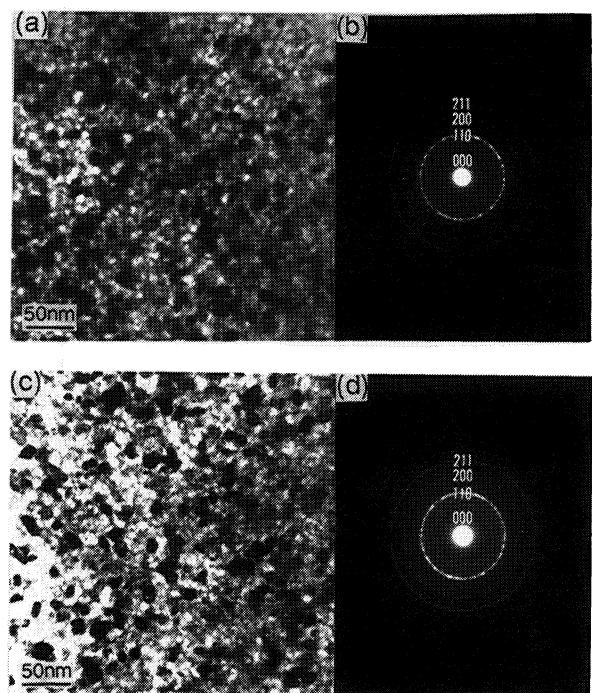

Fig. 8 Bright-field electron micrographs and selected-area electron diffraction patterns of amorphous $Fe_{88}Zr_7B_3Al_2$ (a and b) and $Fe_{86}Zr_7B_3Si_4$ (c and d) alloys annealed for 3.6 ks at 873 K.

Fig. 6 X-ray diffraction patterns of an amorphous $Fe_{88}Zr_7B_3Al_2$ alloy annealed for 3.6 ks at various temperatures.

nearly zero magnetostriction at these alloy compositions as described later.

We further examined the precipitation behavior of the bcc-Fe particles by conventional TEM. Figure 8 shows the bright-field electron micrographs and selected-area electron diffraction patterns of the $Fe_{88}Zr_7B_3Al_2$ and $Fe_{86}Zr_7B_3Si_4$ alloys annealed for 3.6 ks at 873 K. The structure consists mainly of spherical particles with a size of 10 to 20 nm and no appreciable difference in the feature of the microstructure is seen between the Al- and Si-containing alloys. The electron diffraction patterns can be identified to be a bcc-Fe phase with a lattice parameter of about 0.287 nm exceeding that of pure α-Fe for both the alloys, indicating that the nanoscale spherical particles are composed of bcc-Fe phase. Thus, the annealing treatment at the temperatures between the first- and the second-stage exothermic peaks causes the formation of the mixed structure consisting of nanoscale bcc-Fe particles surrounded by the remaining amorphous phase. The distinct identification of the remaining amorphous phase will be presented later.

2. Magnetic properties

Figure 9 shows the change with Al content in the magnetostriction (λ_s), saturation magnetization (B_s) and effective permeability at 1 kHz (μ_e) for the $Fe_{90-x}Zr_7B_3Al_x$ alloys in the as-quenched amorphous and partially crystallized state. The λ_s value of the as-quenched amorphous phase is positive in a whole Al concentration range. The magnitude increases almost linearly from 1×10^{-6} to 7×10^{-6} with increasing Al content from

0 to 10 at% and then beomes saturated in the Al concentration range between 10 and 15 at%. No zero λ_s is obtained for the amorphous phase in the whole Al concentration range. However, the nanoscale bcc-Fe phase obtained by annealing for 3.6 ks at 873 K has a negative λ_s value of -1×10^{-6} at 0 at%Al. The λ_s value passes through zero around 2 at%Al and changes to the positive values with further increasing Al content. The change in λ_s with Al content for the nanoscale bcc Fe alloys takes place almost linearly in the whole Al concentration range of 0 to 15 at%. Here, it is to be noticed that the zero magnetostrictive state is obtained in the vicinity of 2 at%Al for the nanoscale bcc $Fe_{90-x}Zr_7B_3Al_x$ alloys. Considering that the zero magnetostrictive state has not been obtained for the nanoscale bcc Fe-Zr-B ternary alloys[3][4], the replacement of Fe by the small amount of Al is very effective for the achievement of zero λ_s. The similar effect for the achievement of zero λ_s was also observed for the nanoscale bcc $Fe_{90-x}Zr_7B_3Si_x$ alloys. As shown in Fig. 10, the λ_s values for the bcc Fe-Zr-B-Si alloys change from negative values to positive values in the vicinity of 4 at% Si, regardless of B content. The change in λ_s with Si content is different from the result that the as-quenched amorphous alloys have positive λ_s values in the whole Si concentration range. It is further seen that the Si concentration at which the zero λ_s value is obtained shifts to the higher value of Si concentration with increasing T_a. This shift suggests that the Si content in the nanoscale bcc-Fe particles changes with T_a. Additionally, Figs. 9 and 10 show that the B_s of the nanoscale bcc $Fe_{90-x}Zr_7B_3Al_x$ and $Fe_{90-x}Zr_7B_3Si_x$ alloys decreases almost linearly from 1.7 to 1.0 T with increasing Al or Si content from 0 to 15
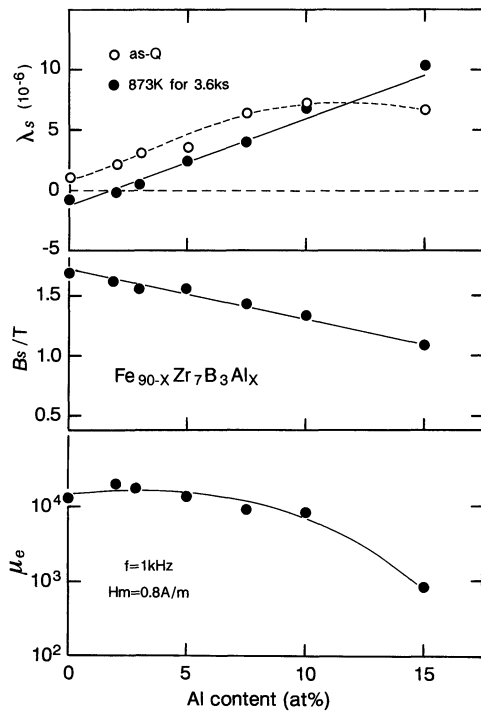

Fig. 9 Changes in magnetostriction (λ_s), saturation magnetization (B_s) and permeability at 1 kHz (μ_e) with aluminum content for amorphous $Fe_{89}Zr_7B_2Al_2$ and $Fe_{88}Zr_7B_3Al_2$ alloys in as-quenched and annealed states.
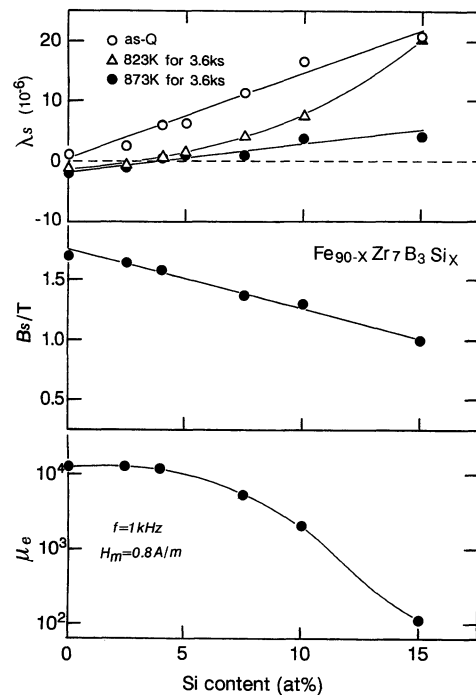
Fig. 10 Changes in λ_s, B_s and μ_e with silicon content for amorphous $Fe_{87}Zr_7B_2Si_4$ and $Fe_{86}Zr_7B_3Si_4$ alloys in as-quenched and annealed states.

at%. On the other hand, μ_e shows a maximum value in the vicinity of 2 at% Al and/or 4 at% Si where zero λ_s value is obtained and then decreases significantly with further increasing Al and/or Si content.

As shown in Figs. 9 and 10, the zero magnetostrictive state has not been obtained for the nanoscale bcc Fe-Zr-B ternary alloys. It is therefore expected that the nanoscale bcc Fe-Zr-B-Al and Fe-Zr-B-Si alloys with nearly zero λ_s exhibit better soft magnetic properties as compared with those for the bcc Fe-Zr-B alloys. Figure 11 shows the changes with T_a in λ_s, B_s and μ_e of the amorphous $Fe_{89}Zr_7B_2Al_2$ and $Fe_{88}Zr_7B_3Al_2$ alloys, along with the results of the crystallized structure and λ_s. Both B_s and μ_e show low values of about 0.5 T and 20, respectively, and λ_s also show large positive values of about 1.8×10^{-6} to 2.7×10^{-6} for the as-quenched amorphous phase. However, the phase transition from the amorphous phase to the nanoscale bcc phase causes the drastic increase in B_s and μ_e values, accompanying the achievement of nearly zero λ_s, and the best combined characteristics of B_s and μ_e are obtained at $T_a = 873$ K corresponding to the temperature just below the precipitation of Fe_3B. Here, it is to be noticed that the good soft magnetic properties of nearly zero λ_s, high μ_e above 10^4 and high B_s above 1.5 T are obtained in the wide T_a range of about 800 to 930 K. The wide T_a range is in contrast to the previous result for the nanoscale bcc $Fe_{90}M_7B_3$ (M=Zr or Hf) alloys[3][4] where the good soft magnetic properties are obtained in the narrow T_a range around 923 K. Thus, one

can notice clearly the effect of the additional Al element on the ease of the synthesis of the nanostructure soft magnetic alloys. The similar changes in λ_s, B_s and μ_e with T_a are also seen for the amorphous $Fe_{87}Zr_7B_2Si_4$ and $Fe_{86}Zr_7B_3Si_4$ alloys, as shown in Fig. 12. The good soft magnetic properties of $\lambda_s \sim 0$, $B_s > 1.5$ T and $\mu_e > 10^4$ are also obtained in the wide T_a range of 823 to 923 K. The highest values of B_s and μ_e which were achieved in the nearly zero λ_s state are 1.61 T and 1.6×10^4, respectively, for the $Fe_{89}Zr_7B_2Al_2$ alloy, 1.61 T and 1.7×10^4, respectively, for the $Fe_{88}Zr_7B_3Al_2$ alloy, 1.56 T and 1.4×10^4, respectively, for the $Fe_{87}Zr_7B_2Si_4$ alloy and 1.55 T and 1.2×10^4, respectively, for the $Fe_{86}Zr_7B_3Si_4$ alloy. These best soft magnetic characteristics are confirmed to be obtained in the nearly zero magnetostrictive state. Furthermore, Fig. 13 shows that the simultaneous addition of Al and Si also causes the achievement of a nearly zero λ_s state for the nanoscale bcc $Fe_{88}Zr_7B_2Si_2Al_1$ and $Fe_{87}Zr_7B_3Si_2Al_1$ alloys annealed for 3.6 ks in the T_a range of 823 to 923 K, accompanying the good soft magnetic properties of $B_s \sim 1.55$ T and $\mu_e > 1.0 \times 10^4$. The nearly zero λ_s value is obtained for the Fe-Zr-B alloy containing 2 at%Si and 1 at%Al and the deviation from the Si and Al concentrations results in the increase in the magnitude of λ_s to negative or positive side. Thus, the nanoscale bcc Fe-Zr-B-Al, Fe-Zr-B-Si and Fe-Zr-B-Si-Al alloys are characterized to have the high B_s of about 1.6 T combined with high μ_e exceeding 1.0×10^4 and nearly zero λ_s at room temperature. The B_s values of the bcc Fe-Zr-B-Al, Fe-Zr-B-Si and Fe-Zr-B-Si-Al al-
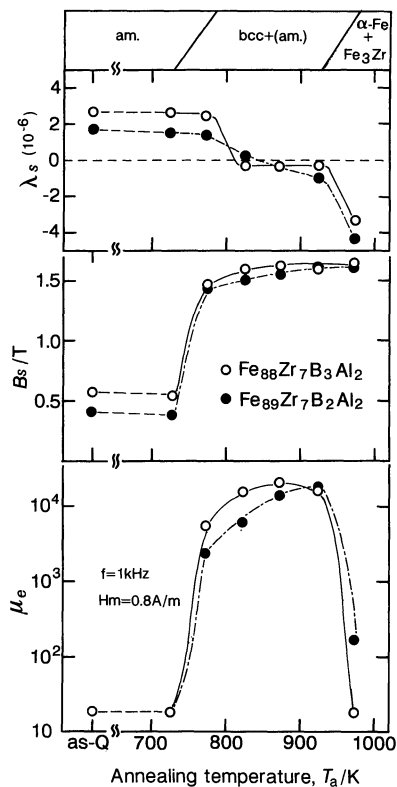

Fig. 11   Changes in λ_s, B_s and μ_e with annealing temperature for amorphous $Fe_{89}Zr_7B_2Al_2$ and $Fe_{88}Zr_7B_3Al_2$ alloys. The data of annealed structure are also shown for reference.
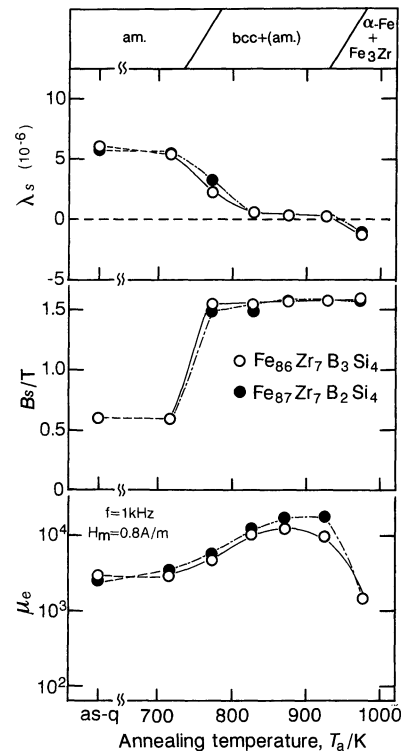
Fig. 12   Changes in λ_s, B_s and μ_e with annealing temperature for amorphous $Fe_{87}Zr_7B_2Si_4$ and $Fe_{86}Zr_7B_3Si_4$ alloys. The data of annealed structure are also shown for reference.
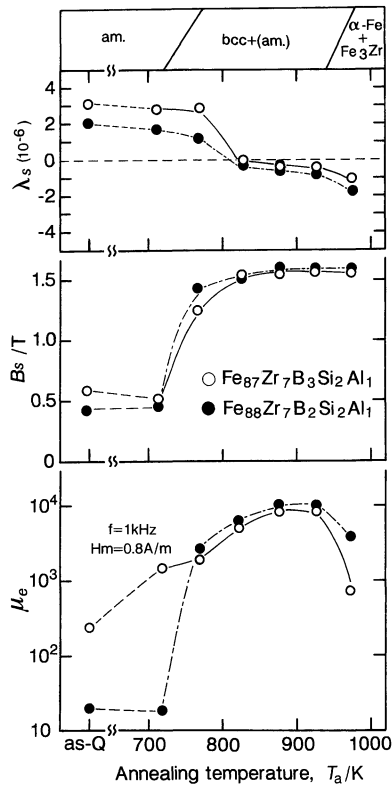
Fig. 13 Changes in λ_s, B_s and μ_e at 1 kHz with annealing temperature for amorphous $Fe_{88}Zr_7B_2Si_2Al_1$ and $Fe_{87}Zr_7B_3Si_2Al_1$ alloys. The data of annealed structure are also shown for reference.

Fig. 14 High-resolution TEM image (a) and nanobeam electron diffraction patterns (b) and (c) taken from the regions with a diameter of 3 nm marked with A and B for an amorphous $Fe_{88}Zr_7B_3Al_2$ alloy annealed for 3.6 ks at 873 K. The diffraction pattern (b) and (c) are identified to be (111) of the bcc-Fe phase and amorphous phase, respectively.

loys are considerably higher than those of the Fe–Si–B–Nb–Cu[2] and Fe–Si–B–Nb–Ga[5] alloys and comparable to those for the Fe–M–B alloys[3][4] It is generally known that μ_e is strongly sensitive to the sample shape because of the influence of demagnetizing fields. Although the present μ_e values are obtained from the melt-spun ribbons with a width of 1 mm, their values are expected to increase significantly by the use of circular ring-shape samples which are prepared by mechanical punching amorphous Fe–Zr–B–Al, Fe–Zr–B–Si and Fe–Zr–B–Si–Al sheets with a much wider width above 10 mm.

3. High-resolution TEM image and nanobeam composition analyses

The best combined characteristics of high B_s, high μ_e and zero λ_s are obtained in the nanoscale mixed structure consisting of nanoscale bcc particles with a size of 10 to 20 nm embedded in the amorphous matrix. It is therefore important to clarify the dispersion state of the bcc-Fe particles in the amorphous matrix and the solute compositions of the bcc and amorphous phases. Figure 14 shows the high-resolution TEM image and the nanobeam electron diffraction patterns taken from the regions A and B for the bcc $Fe_{88}Zr_7B_3Al_2$ alloy obtained by annealing for 3.6 ks at 873 K. Nearly spherical bcc-Fe particles with an average diameter of about 15 nm are always surrounded by the amorphous phase with an average thickness of about 10 nm. The nanobeam diffraction patterns taken from the regions A and B with a diameter of 3 nm are
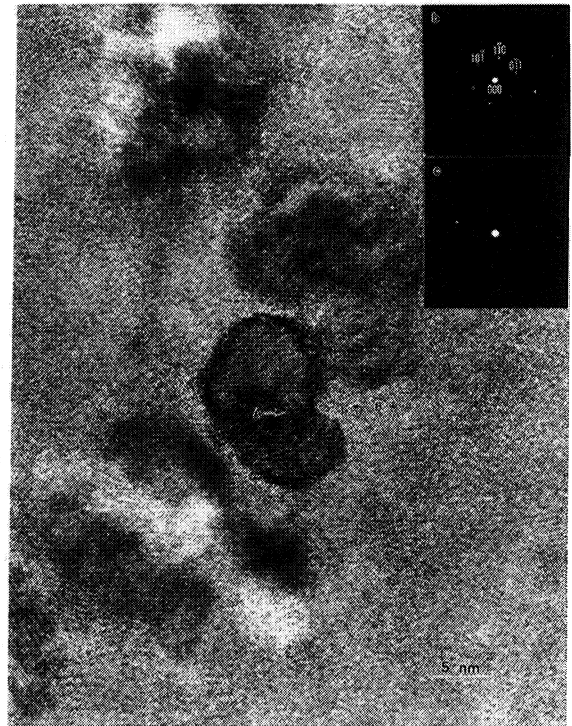
identified as the bcc and amorphous phases, respectively, indicating clearly that the nanoscale particles have a bcc structure. The nanobeam EDX spectroscopic profiles taken from the bcc-Fe and remaining amorphous phase are shown in Fig. 15, where the analytical constituent ratios among Fe, Zr and Al except B are also presented. The accuracy of the analytical solute concentration obtained by EDX spectrometry using a Fe-3.5 mass%Si alloy as the standard specimen was evaluated within 0.3 at%. The analytical Zr and Al concentrations of the $Fe_{88}Zr_7B_3Al_2$ alloy are 4.1 and 2.6 at% respectively, for the bcc particle and 12.2 and 1.3 at%, respectively, for the amorphous phase. The analytical data indicate that the Al element is enriched into the bcc-Fe phase while the Zr element is excluded from the bcc-Fe phase and segregated to the remaining amorphous phase. Considering that the nanoscale bcc phase in the $Fe_{90}Zr_7B_3$ alloy has the negative λ_s of 1×10^{-6}, the simultaneous dissolution of about 3 at% Al and 4 at%Zr is said to be neccessary for the achievement of zero λ_s. Furthermore, the enrichment of Zr to the remaining amorphous phase causes the increase in thermal stability of the amorphous phase which is important for the formation of the nanoscale mixed structure.

The formation of the similar nanoscale mixed structure consisting of bcc-Fe and Zr-rich amorphous phase is confirmed for the $Fe_{86}Zr_7B_3Si_4$ alloy from the high-resolution TEM image and nanobeam electron diffraction pat-
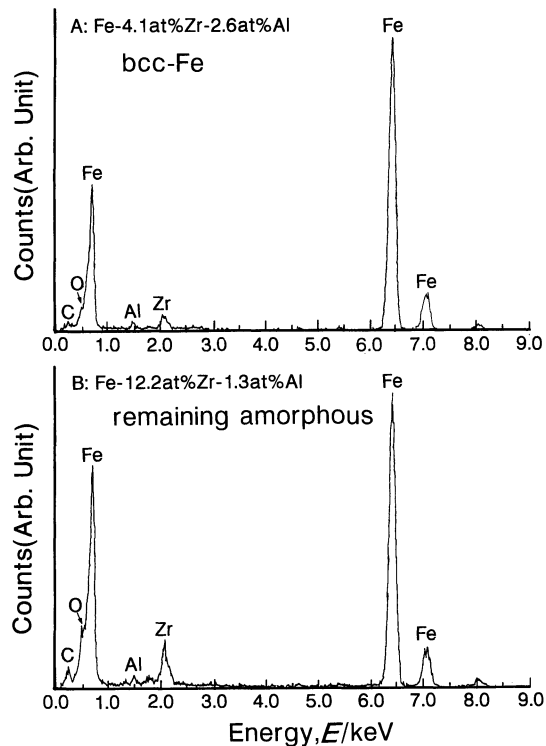
Fig. 15   Energy dispersive X-ray spectroscopy (EDX) profiles (a) and (b) taken from regions A and B, respectively, in Fig. 14(a) for an amorphous $Fe_{88}Zr_7B_3Al_2$ alloy annealed for 3.6 ks at 873 K.
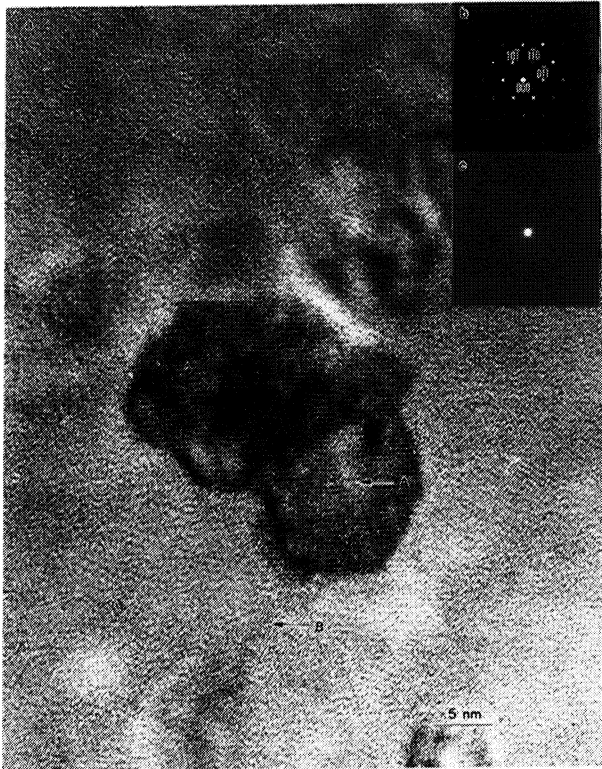

Fig. 16   High-resolution TEM image (a) and nanobeam electron diffraction patterns (b) and (c) taken from the regions with a diameter of 3 nm marked with A and B for an amorphous $Fe_{86}Zr_7B_3Si_4$ alloy annealed for 3.6 ks at 873 K. The diffraction pattern (b) and (c) are identified to be (111) of the bcc-Fe phase and amorphous phase, respectively.

terns, as shown in Fig. 16. It is seen that the bcc-Fe particles with an average particle size of about 18 nm disperse homogeneously and isolately in the amorphous phase with an average interparticle spacing of about 9 nm. No distinct difference in the nanoscale mixed structure is seen between the Al- and the Si-containing alloys. The solute concentration was analyzed to be 2.0 at% Zr and 6.3 at% Si for the bcc-Fe particle and 10.5 at% Zr and 3.1 at% Si for the remaining amorphous phase. Since no information on B was obtained in the EDX spectroscopy analysis, the evaluation of the solute composition was made in the assumption that the Fe-Zr-B-Si alloy does not contain the B element. It is again confirmed that the Si element is enriched to the bcc-Fe phase while the Zr element is excluded from the bcc-Fe phase to the remaining amorphous phase. These nanoscale analytical data allow us to conclude that the nanoscale bcc-Fe particles exhibiting the nearly zero λ_s are composed of Fe-2.6 at%Al or Fe-6.3 at%Si phase containing about 2 to 4 at% Zr.

IV. Discussion

1. Reasons for the formation of nanoscale bcc structure and the achievement of good soft magnetic properties

Based on the previous discussion on the microstructure and soft magnetic properties of nanocrystalline Fe-Si-B-Nb-Cu[2] and Fe-M-B (M=Zr, Hf or Nb)[3][4] alloys, we can presume that the good soft magnetic properties for the present nanoscale bcc alloys in Fe-Zr-B-Al and Fe-Zr-B-Si systems are attributed to the combination of (1) the disappearance of apparent crystallomagnetic anisotropy resulting from the homogeneous dispersion of spherical bcc particles, (2) the ease of reversion of magnetic domain walls because the size of the bcc grains is much smaller than the size of domain walls, (3) the achievement of high B_s through magnetic coupling among the nanoscale bcc particles via ferromagnetic amorphous phase with nanoscale interparticle spacing, (4) the achievement of zero λ_s through the redistribution of solute elements between the bcc phase and the remaining amorphous phase, and (5) the maintenance of nanoscale bcc structure in a wide temperature range resulting from the high thermal stability of the remaining amorphous phase. When the simultaneous achievement of these factors is assumed to be the reason for the good soft magnetic properties, the achievement is attributed to the formation of the nanoscale bcc structure in the wide temperature range. Furthermore, the key factor for the formation of the crystallization-induced nanostructure which enables the magnetic exchange coupling leading to the appearance of the high magnetization is the residual existence of the amorphous phase as the intergranular phase. It is therefore important to investigate the reason why the remaining amorphous phase has high thermal stability and causes the formation of the nanoscale mixed structure. It is confirmed in Fig. 15 that the Zr element is significantly enriched in the intergranular amorphous

phase. It is also known that the crystallization tempera-
ture of the Fe–Zr–B amorphous alloys increases sig-
nificantly with increasing Zr and B contents[13]. The ana-
lytical Zr concentration in the remaining amorphous
phase has been reported to be about 10 to 20 at%[14][15]. It
is therefore estimated that the crystallization temperature
increases from 769 K for the $Fe_{91}Zr_7B_2$ alloy to 868 K for
the remaining amorphous $Fe_{82}Zr_{12}B_6$, from the previous
data on the compositional dependence of crystallization
temperature[13] for Fe–Zr–B amorphous alloys. There are
no data available on the crystallization temperature of
Fe–Zr–B–Al and Fe–Zr–B–Si alloys. However, the Al
and Si are enriched to the bcc phase and the influence of
Al or Si element on the thermal stability of the remaining
amorphous phase is less significant. Furthermore, in the
present study, we do not have any data of B concentra-
tion in the remaining amorphous phase. More recently,
the atom probe field ion microscopy (AP-FIM) study was
carried out for the nanocrystalline bcc alloys in the
$Fe_{90}Zr_7B_3$ alloy and the B element was confirmed to
be significantly enriched into the amorphous phase[15].
Therefore, it is reasonable to consider that the remaining
amorphous phase has a crystallization temperature much
higher than 868 K for the $Fe_{82}Zr_{12}B_6$ alloy. The crystalliza-
tion temperature estimated thus is consistent with the
present result that the amorphous phase is maintained
even after annealing for 3.6 ks at 923 K. Based on the re-
cent data[15] on the distribution of the solute elements in
nanoscale bcc $Fe_{90}Zr_7B_3$ alloy obtained by AP-FIM, the
solute distribution profiles of Zr, B and Al or Si elements
in the nanoscale bcc Fe–Zr–B–Al and Fe–Zr–B–Si alloys
are schematically illustrated in Fig. 17, together with the
data on nanoscale bcc and amorphous phases in Fe–Zr–
B[15] alloys. The Zr and B elements in the Fe–Zr–B system
do not distribute homogeneously in the intergranular
amorphous phase and are enriched more significantly in

the vicinity of the interface between the amorphous and
bcc-Fe phases. Besides, the solute element which is effec-
tive for the appearance of the steep concentration
gradient near the interface has been reported[16] to satisfy
with the following four criteria; (1) high melting tempera-
ture, (2) large atomic size or large atomic size ratio
among the constituent elements, (3) large negative heat
of mixing against the major element, and (4) nearly zero
solubility limit against the major element. These criteria
are satisfied for Zr and B elemnets in Fe–Zr–B–Al and
Fe–Zr–B–Si systems. Consequently, the steep gradient
distribution of the Zr and B elements is also expected to
occur in the present intergranular amorphous phase for
the present alloys, as illustrated in Fig. 17. As a result,
the thermal stability of the remaining amorphous phase
is expected to increase through the combination of the
following four effects[16]; (1) high gradient effect leading
to the increase in thermal stability of an amorphous
phase, (2) suppression of grain growth leading to the
homogeneous dispersion of nanocrystalline particles, (3)
suppression of heterogeneous nucleation at the interface
between crystalline particle and amorphous matrix, and
(4) gradual redistribution of alloy components among
the constituent phases. It is therefore concluded that the
present good soft magnetic properties combined with
high B_s originate from the unique partial crystallization
leading to the nanoscale mixed phases with particle sizes
and alloy components which are appropriate for the
appearance of soft magnetism through the remaining
amorphous phase.

2. Reason for the achievement of zero magnetostriction

The high-resolution TEM and nanobeam composition
analyses in Figs. 14 to 16 indicate that the nanoscale bcc
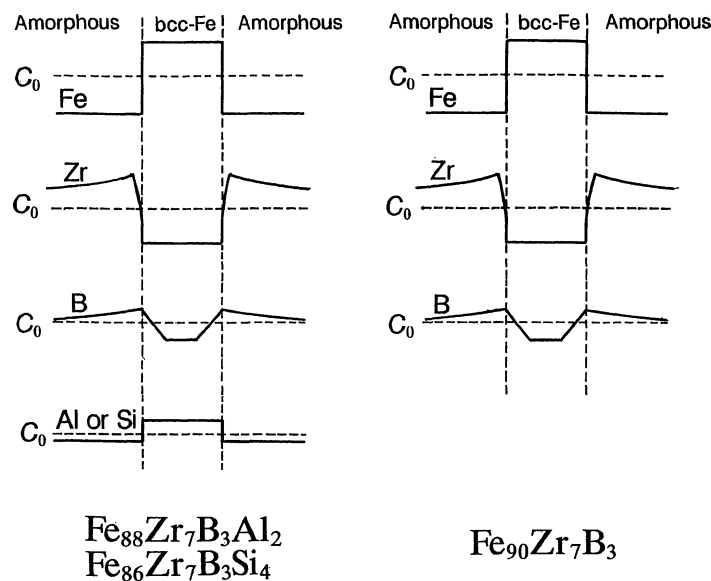particles surrounded by the remaining amorphous phase

Fig. 17   Schematic illustration of the concentration profiles of Zr, B and Al or Si elements across the interface between bcc-Fe
and remaining amorphous phase in the amorphous $Fe_{88}Zr_7B_3Al_2$ and $Fe_{86}Zr_7B_3Si_4$ alloys annealed for 3.6 ks at 873 K. The
previous data of a partially crystallized $Fe_{90}Zr_7B_3$ alloy taken from Ref. (15) are also shown for reference.

are not a pure α-Fe phase but a solid solution containing the Zr and Al or Si elements. Although the analytical compositions of the bcc and amorphous phases obtained by EDX spectrometry have the error of 0.3 at%, the Zr and Al or Si concentrations are determined to be 4.6 at% Zr and 2.6 at%Al for the bcc phase and 12.2%Zr and 1.3%Al for the remaining amorphous phase in the nanocrystalline $Fe_{88}Zr_7B_3Al_2$ alloy and 2.0%Zr and 6.3%Si for the bcc phase and 10.5%Zr and 3.1%Si for the remaining amorphous phase in the nanocrystalline $Fe_{86}Zr_7B_3Si_4$ alloy. One can see a clear tendency that the Al or Si element is enriched to the bcc phase while the Zr concentration is excluded from the bcc phase to the remaining amorphous phase. Here, it is important to point out that the bcc particles contain simultaneously Zr and Al or Si elements. There are no data on the compositional dependence of λ_s for Fe–Zr–Al and Fe–Zr–Si alloys consisting only of a bcc phase. It is generally known that the λ_s value is negative for pure bcc-Fe metal[17] and the dissolution of Zr, Al and Si into bcc-Fe phase causes the decrease in the magnitude of negative λ_s value, leading to zero λ_s for bcc Fe-5 mass%Al[18] and Fe-6.5 mass% Si[19] alloys. From the change in λ_s of bcc Fe phase with Zr, Al or Si content shown in Figs. 9 and 10, we can expect that zero λ_s value of bcc-Fe phase is obtained at lower solute concentration side by the simultaneous dissolution of Zr, Al and Si elements into bcc Fe phase. It is therefore concluded that the present achievement of zero λ_s value at the lower Al or Si solute concentration as compared with those for the binary Fe–Al and Fe–Si alloys is due to the simultaneous dissolution of Zr and Al or Si elements resulting from the formation of metastable bcc-Fe phase. Thus, the formation of the metastable bcc solid solution with compositions, which cannot be obtained in an equilibrium state, is very interesting for future development of new functional materials including magnetic material.

3. Glass formation in the Fe–Zr–B–Al and Fe–Zr–B–Si systems

We investigate the effect of the addition of Al or Si on the glass formation tendency of Fe–Zr–B alloys. Since the nanoscale bcc structure in Fe–Zr–B ternary system has good soft magnetic properties, it is important to find an additional element which is effective for the increase in the glass-forming ability without detriment to good soft magnetic properties. It is shown in Section III-1 that the maximum sample thickness for glass formation increases from about 18 μm for $Fe_{90}Zr_7B_3$ to about 26 μm for $Fe_{88}Zr_7B_3Al_2$ and about 28 μm for $Fe_{86}Zr_7B_3Si_4$, accompanying the increase in μ_e and the achievement of zero λ_s. It has previously been reported that an amorphous phase is formed in rapidly solidified ternary alloys of Fe–Zr–B[13] Fe–B–Al[20] and Fe–B–Si[21] systems. Based on the previous data on the glass formation range and the maximum sample thickness of their amorphous alloys, it is concluded that the glass-forming ability decreases in the order Fe–B–Si > Fe–B–Al > Fe–Zr–B. This order suggests that the effectiveness of the addition-

al element on the glass-forming ability of the Fe–B base alloys decreases in the order Si > Al > Zr. Consequently, the addition of Si or Al which has the effectiveness exceeding Zr is thought to cause the increase in the glass-forming ability of Fe–Zr–B alloys.

Here, it is important to discuss the reason why the effectiveness of additional element on the glass-forming ability of the Fe–B base alloys decreases in the order Si > Al > Zr. Although the glass-forming ability is closely related to the atomic size and bonding state among the constituent elements, it is rather difficult to compare the glass-forming ability directly among the three elements, because of the difference in metal and metalloid. However, when we look at the melting temperatures of Fe-based binary alloys in Fe–B, Fe–Si, Fe–Al and Fe–Zr systems and the Zr-based binary alloys in Zr–B, Zr–Si and Zr–Al systems, the melting temperature decreases in the order Fe–Zr > Fe–Al > Fe–Si > Fe–B for the former system and Zr–Si > Zr–Al > Zr–B for the latter system[10]. No data available on the equilibrium phase diagrams of these ternary alloys have been presented. However, the melting temperatures were measured to decrease in the order of Fe–B–Zr > Fe–B–Al > Fe–B–Si from differential thermal analytical data[22]. It is generally recognized that the glass-forming ability in the same Fe–B base alloys such as Fe–B–M (M=Zr, Al or Si) tends to increase with decreasing melting temperature. Consequently, the difference in melting temperatures among the three Fe base alloys seems to cause the change in the glass-forming ability in the order Fe–B–Si > Fe–B–Al > Fe–B–Zr. As a result, we can detect that the effect of additional M elements on the glass-forming ability of the Fe–B–M ternary alloys is the largest for Si, followed by Al and then Zr.

V. Summary

We have examined the possibility that the addition of a small amount of Al and/or Si to $Fe_{91}Zr_7B_2$ and $Fe_{90}Zr_7B_3$ alloys causes the formation of a nanoscale bcc structure by annealing the rapidly solidified Fe–Zr–B–Al, Fe–Zr–B–Si and Fe–Zr–B–Al–Si amorphous alloys and the achievement of zero λ_s and the improvement of soft magnetic properties for the resulting nanoscale bcc Fe–Zr–B–(Al, Si) alloys. The results obtained are summarized as follows:

(1) An amorphous single phase was formed in the whole composition ranges of $Fe_{91-x}Zr_7B_2Al_x$, $Fe_{90-x}Zr_7B_3Al_x$, $Fe_{91-x}Zr_7B_2Si_x$ and $Fe_{90-x}Zr_7B_3Si_x$ ($x=0$ to 15 at%) by rapid solidification. The maximum ribbon thickness for glass formation increases from about 18 μm for $Fe_{90}Zr_7B_3$ to about 26 μm for $Fe_{75}Zr_7B_3Al_{15}$ and about 28 μm for $Fe_{75}Zr_7B_3Si_{15}$.

(2) The onset temperature of crystallization increases from 780 K for $Fe_{90}Zr_7B_3$ to 820 K for $Fe_{75}Zr_7B_3Al_{15}$ and 814 K for $Fe_{75}Zr_7B_3Si_{15}$. Thus, the thermal stability of the amorphous phase increases significantly by the addition of Al or Si.

(3) The crystallization takes place through two stages of Am→Am+bcc-Fe→bcc-Fe+Fe_3Zr, regardless of Al

and Si contents. By annealing at temperatures between the first and the second reactions, the nanoscale bcc structure in coexistent with the remaining amorphous phase is obtained. The bcc phase has the spherical morphology with an average particle size of about 15 nm and disperse in an amorphous matrix at an average interparticle spacing of about 10 nm. The nanobeam compositional analyses indicate that the bcc-Fe phase contains about 2 to 4%Zr and 3%Al or 6%Si. The Zr element was enriched to the remaining amorphous phase and the composition was analyzed to be about 11 to 12%Zr and 1%Al or 3% Si. The enrichment of Zr is the dominant factor for the maintenance of the nanoscale bcc structure through the increase in thermal stability of the remaining amorphous phase.

(4) The λ_s value of the nanoscale bcc phase is negative for the $Fe_{91}Zr_7B_2$ and $Fe_{90}Zr_7B_3$ alloys. The replacement of Fe by Al and/or Si causes the change of λ_s from negative to positive value through zero around 2 at%Al, 4 at%Si or 2 at%Si+1 at%Al. The achievement of the zero λ_s at the lower Al and/or Si content was interpreted to be due to the simultaneous dissolution of Zr and Al and/or Si.

(5) The highest μ_e was obtained for $Fe_{89}Zr_7B_2Al_2$, $Fe_{87}Zr_7B_2Si_4$ and $Fe_{88}Zr_7B_2Si_2Al_1$ with zero λ_s. The μ_e at 1 kHz and B_s are 1.7×10^4 and 1.61 T, respectively, for the Al-containing alloy, 1.4×10^4 and 1.56 T, respectively, for the Si-containing alloy and 1.2×10^4 and 1.55 T, respectively, for the Si- and Al-containing alloy. It is thus concluded that the addition of a small amount of Al and/or Si to the nanoscale bcc Fe–Zr–B alloys is effective for the increase in μ_e through the achievement of zero λ_s.

REFERENCES

(1) Proc. of the 2nd Int. Conf. on Nanostructured Materials (NANO' 94), ed. by H. E. Schaefer *et al.*, Stuttgart, (1995).
(2) Y. Yoshizawa, S. Oguma and K. Yamauchi: J. Appl. Phys., **64** (1988), 6044.
(3) K. Suzuki, N. Kataoka, A. Inoue, A. Makino and T. Masumoto: Mater. Trans., JIM, **32** (1990), 743.
(4) K. Suzuki, A. Makino, N. Kataoka, A. Inoue and T. Masumoto: Mater. Trans., JIM, **33** (1991), 93.
(5) T. Tomida: Mater. Sci. Eng., A179/A180 (1994), 521.
(6) A. Makino, A. Inoue and T. Masumoto: Collected Abstracts of 1995 Annual Spring Meeting of Japan Inst. Metals.
(7) K. Hono, K. Hiraga, Q. Wang, A. Inoue and T. Sakurai: Acta Metall. et Mater., **40** (1992), 2137.
(8) A. Makino, A. Inoue and T. Masumoto: Nanostructured Materials, **6** (1995), 985.
(9) A. Inoue, Y. Miyauchi and T. Masumoto: Mater. Trans., JIM, **36** (1995), 689.
(10) *Metals Databook*, ed. by Japan Inst. Metals, Maruzen, Tokyo, (1983), p. 41.
(11) *Binary Alloy Phase Diagrams*, ed. by T. B. Massalskii, ASM Intern., Materials Park, Ohio (1990).
(12) F. R. de Boer, R. Boom, W. C. M. Mattens, A. R. Miedema and A. K. Niessen: *Cohesion in Metals*, Vol. 1, North-Holland, Amsterdam (1988).
(13) A. Inoue, K. Kobayashi, M. Nose and T. Masumoto: J. Physique, Colloque, C8 (1980), 831.
(14) A. Makino, K. Suzuki, A. Inoue and T. Masumoto: Mater. Sci. Eng., A179/A180 (1994), 127.
(15) Y. Zhang, K. Hono, A. Inoue, A. Makino and T. Sakurai: Acta Met., in press.
(16) A. Inoue, A. Takeuchi, A. Makino and T. Masumoto: Mater. Trans., JIM, **36** (1995), 676.
(17) E. W. Lee: Rep. Prog. Phys., **18** (1955), 184.
(18) H. Masumoto and T. Yamamoto: J. Japan Inst. Metals, **1** (1937), 127.
(19) M. F. Littmann: IEEE Trans. Mag., **MAG-7** (1971), 48.
(20) A. Inoue, A. Kitamura and T. Masumoto: J. Mater. Sci., **16** (1981), 1895.
(21) A. Inoue, T. Masumoto, M. Kikuchi and T. Minemura: J. Japan Inst. Metals, **42** (1978), 294.
(22) Y. Miyauchi, A. Inoue and A. Makino: unpublished research (1994).